Some Aspects of Vortex Structure Related to Tropical Cyclone Motion

MICHAEL FIORINO*

Fleet Numerical Oceanography Center, Monterey, California

RUSSELL L. ELSBERRY

Department of Meteorology, Naval Postgraduate School, Monterey, California

(Manuscript received 6 June 1988, in final form 13 October 1988)

ABSTRACT

Some effects of tropical cyclone structure on the vortex motion are examined in a nondivergent, barotropic numerical model with no basic current. As suggested earlier by DeMaria, the initial maximum wind speed has little effect on the track. Vortex translation associated with the beta effect depends sensitively on the strength of the flow between 300 and 1000 km from the center. If the flow in this annulus is made more cyclonic, the track will turn cyclonically and move more toward the west in the Northern Hemisphere.

The dynamics of this beta-drift is studied via a decomposition into symmetric and asymmetric circulations. The symmetric flow experiences a slight weakening of the maximum wind speed and an anticyclonic circulation is induced beyond 600 km. The asymmetric circulation is dominated by an azimuthal wavenumber one circulation with an anticyclonic gyre east of the center, a cyclonic gyre to the west and a nearly uniform, broad-scale ventilation flow between the gyres. The vortex translation speed and direction are almost equal to the average of this ventilation flow over the area of significant cyclonic circulation in the vortex.

Analysis of the model streamfunction tendency equation demonstrates that the linear beta term is responsible for the initial formation of the asymmetric gyres. Nonlinear advection of the asymmetric circulation by the symmetric vortex flow twists the interior region between the gyres and orients the ventilation flow toward the northwest rather than toward the north. Because this term nearly balances the linear beta forcing, the streamfunction time tendency (and storm motion) is predominantly due to the advection of the symmetric vortex by the ventilation flow between the gyres.

1. Introduction

The dominant concept in the theory and forecasting of tropical cyclone motion is "steering" by an assumed uniform flow. For example, the observational studies of George and Gray (1976) and Brand et al. (1981) clearly show a relationship between the mean (over many storm cases) tropical cyclone motion vector and a mean steering flow vector. However, Neumann (1979) illustrates the difficulties in defining the horizontal steering current and at what level the steering process is operating. Perhaps the lack of adequate observations in the region of tropical cyclones is a significant contributor to the uncertainties in the tropical cyclone-steering relationship. Moreover, tropical cyclone motion should be expected to be more complex than a simple relationship to some mean flow at a single (or integrated) level. First, the separation of the tropical cyclone scale of motion from that of the "environment" is not as simple and clear-cut as steering theory would imply. More importantly, the tropical cyclone is not a solid vortex that is being pushed along by some "steering" stream. In reality, the storm interacts with its environment in many ways. Therefore, the fundamental physical problem is how this interaction occurs. The particular goal of this study is to understand how the structure of the tropical cyclone contributes to this interaction, and thus to the motion.

Observational studies of the dependence of motion on tropical cyclone structure have been mainly based on composite studies. The most notable is by Chan (1982), who showed systematic differences between the steering flow vector and the storm motion vector as a function of cyclone size (defined as the radius of 30 kt or 15 m s^{-1} winds) and intensity (defined as the maximum wind speed).

Early theoretical studies of tropical cyclone motion assumed very simple models for the cyclone structure. Although the poleward drift of a symmetric, cyclonic vortex in solid body rotation was first deduced by Ferrel (1859), this discovery is commonly attributed to Rossby (1948). Other examples of the use of a solid body rotation vortex model include Yeh (1950) and Kuo (1969).

* Present affiliation: Evans Communications, Inc., Arlington, VA.

Corresponding author address: Dr. Michael Fiorino, 3406 Estonia Dr., Bowie, MD 20716.

Significant improvements in tropical cyclone motion theories occurred in the 1950s, as highlighted by the work of Kasahara (1957). Although the motion solutions were derived from a physically more realistic basis, the only dependency on storm structure was represented by a size parameter. Extensions of these barotropic, analytical theories to a baroclinic atmosphere (Kasahara 1960) did not address the role of structure in the motion processes.

Recent developments have expanded and clarified the problem. Holland (1983) and Chan (1982) analytically solved the barotropic vorticity equation with a vortex profile that more explicitly demonstrated how cyclone size influences motion under simple environmental flow conditions. DeMaria (1985) examined the same problem with a spectral barotropic model. With this spectral approach, it is not necessary to linearize the nonlinear advection term by assuming a small perturbation in a large-scale environment as is necessary in analytical treatments. Furthermore, the inherent aliasing of finite difference models is reduced in a spectral model. While DeMaria's results tended to confirm the findings from the simpler models, he also demonstrated that the impact of storm size on motion was a function of the base state (large-scale flow) vorticity gradient.

More recently, Chan and Williams (1987) have examined in more detail the underlying barotropic dynamics of tropical cyclone motion. They have shown that the nonlinear advection terms in the barotropic vorticity equation are required for significant displacement of the vortex center. The primary role of the so-called β (latitudinal gradient of Coriolis parameter) term is to force a wavenumber one asymmetric distortion in the initially symmetric vortex by Rossby wave dispersion. However, the linear β effect does not cause significant translation of the storm center. Rather, the storm is advected primarily by the linearly induced asymmetric circulation. Structural effects were examined by fixing the shape of the tangential wind profile and varying the maximum winds. They demonstrated that larger storms have greater motion, or "beta-drift", in their no uniform flow experiment.

Experimentation with baroclinic numerical models has been surprisingly limited. Mathur (1987) has inserted different vortex structures into a sophisticated hurricane model and found sensitivity to cyclone size.

The basic goals of this research are:

(i) To more completely understand the dynamics of the barotropic motion processes; and

(ii) To determine which features of the vortex (e.g., maximum wind, size, total relative angular momentum, etc.) have the greatest influence on motion.

The nondivergent barotropic numerical model used in this research will be described in the next section. The dependence of the beta-drift on the initial symmetric vortex structure will then be illustrated by specifying various tangential wind profiles. The dynamics of beta drift is then examined through a streamfunction tendency analysis of the symmetric and asymmetric circulations. This analysis explicitly demonstrates how the symmetrical circulation induces an asymmetric flow via linear Rossby wave dispersion and how the asymmetric circulation interacts with the symmetric circulation to move the vortex. A fundamental result of this study is that the dynamics of tropical cyclone motion are highly nonlinear and that the initial (and evolving) vortex structure can be a large factor in the beta-drift.

2. The numerical model

The dynamical basis of this study is the conservation of absolute vorticity, which is mathematically expressed by the nondivergent barotropic vorticity equation. This model contains two fundamental dynamical processes involved in vortex motion: (i) nonlinear interaction (advection) and (ii) linear wave dispersion due to the gradient of absolute vorticity (i.e., the β effect). Both processes are critical to motion as recently shown by Chan and Williams (1987) and by a number of earlier studies (e.g., Adem 1956).

Assuming that β is a constant (the β-plane approximation), the governing equation for the relative vorticity (ζ) is

$$\frac{\partial \zeta}{\partial t} + \mathbf{V} \cdot \nabla \zeta + \beta v = 0. \tag{1}$$

In this study, β is set to a value valid at 15°N. The assumption that absolute vorticity is conserved implies that the flow is nondivergent. Thus, a streamfunction (ψ) can be defined to represent the wind components. That is,

$$\nabla^2 \psi = \zeta, \tag{2}$$

$$\mathbf{V} = \mathbf{k} \times \nabla \psi, \quad \text{or} \quad u = -\frac{\partial \psi}{\partial y}, \quad v = \frac{\partial \psi}{\partial x}. \tag{3}$$

Applying the streamfunction representation to (1) and rearranging the order of differentiation, the model equation to be solved numerically is

$$\nabla^2 \frac{\partial \psi}{\partial t} + J(\psi, \nabla^2 \psi) + \beta \frac{\partial \psi}{\partial x} = 0, \tag{4}$$

where J is the Jacobian defined as

$$J(\psi, \nabla^2 \psi) = \frac{\partial \psi}{\partial x}\frac{\partial \zeta}{\partial y} - \frac{\partial \psi}{\partial y}\frac{\partial \zeta}{\partial x} = v \frac{\partial \zeta}{\partial y} + u \frac{\partial \zeta}{\partial x}. \tag{5}$$

Thus, changes in ψ are due to both nonlinear ($J\{\psi, \nabla^2\psi\}$) and linear ($\beta \partial\psi/\partial x$) effects. Setting the Jacobian term to zero produces the linear vorticity equation that describes pure Rossby wave dispersion.

The model equation (4) is solved on a rectangular, Cartesian grid with uniform grid spacing. A typical

configuration is 101 × 101 points in the north–south and east–west directions with a horizontal grid increment of 40 km. The Jacobian term is estimated using the Arakawa (1966) form, which ensures conservation of energy and enstrophy, and the linear β term is calculated using centered differences. Given the forcing function on the right-hand side of (4), the Helmholtz equation for the streamfunction tendency is solved using a direct or matrix inversion method.

The omission of a basic current in this study greatly simplifies the interpretation of the results and allows application of simple boundary conditions. The lateral boundary conditions are no slip (zero gradient in ψ) along the northern and southern boundaries, and cyclic continuity in the east–west direction. With these boundary conditions (and a constant β), it is quite simple to move the grid to keep the translating storm center near the middle of the grid. When the vortex center moves one grid interval away from the grid center, the indices of the solution are shifted one value in the opposite direction. For example, if the vortex center moved westward from $I = 51$ to $I = 50$, then the $I = 1$ ($I = 100$) value on the unshifted grid becomes the $I = 2$ ($I = 101$) value on the shifted grid. The cyclic ψ boundary conditions then may be applied to specify the solution on the leading edge of the shifted grid. The record of the grid shifts allows reconstruction of the vortex track relative to a fixed grid. Experiments with moving and stationary grids showed very little difference (less than 1%) in the tracks.

3. Effect of the initial symmetric vortex on the motion

The dependence of motion on the initial symmetric structure of the vortex will be described via a series of initial condition sensitivity tests. The examples of initial symmetric wind profiles in Fig. 1 are based on the analytical tangential wind profile of Chan and Williams (1987)

$$v(r) = V_{\max}\left[\frac{r}{r_{\max}}\right]\exp\left\{\frac{1}{b}\left[1-\left[\frac{r}{r_{\max}}\right]^b\right]\right\}, \quad (6)$$

where $v(r)$ is the tangential wind, $V_{\max}$ is the maximum wind (intensity), $r_{\max}$ is the radius of maximum wind and b is an exponential factor that together with $r_{\max}$ governs the shape of the profile outside $r = r_{\max}$. Such a profile is fitted to specific size (radius of 15 m s^{-1} winds) and intensity values by calculating the b factor for a smooth profile passing through two specified v values at $r = r_{\max}$ and at a larger radius r_1. Given ($V_{\max}$, $r_{\max}$) and the outer pair (v_1, r_1), the solution for b is

$$\ln\left[\frac{v_1}{V_{\max}}\cdot\frac{r_{\max}}{r_1}\right] = \frac{1}{b}\left[1-\left[\frac{r}{r_{\max}}\right]^b\right]. \quad (7)$$

This equation is solved numerically using modified linear interpolation (Gerald and Wheatley 1984). For example, b is equal to 0.96 for the profile in Fig. 1 that has $V_{\max} = 35$ m s^{-1}, $R_{\max} = 100$ km, $v_1 = 15$ m s^{-1} and $r_1 = 300$ km. The profile using this numerically determined b comes within 0.01 m s^{-1} of v_1 at r_1.

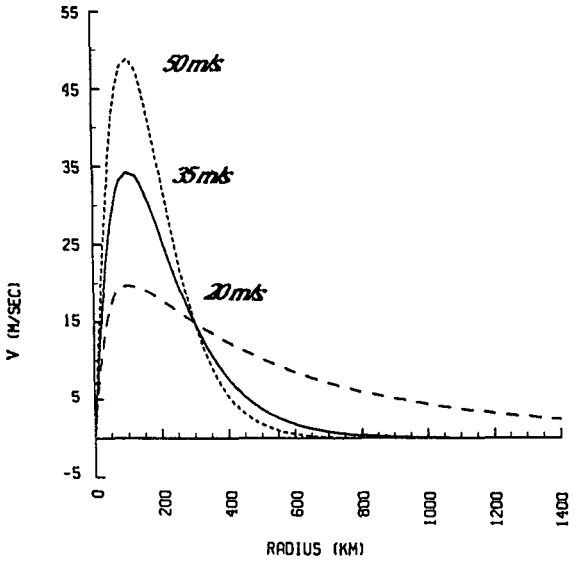

FIG. 1. Tangential wind profiles of three vortices with intensities of 50 m s^{-1} (short-dashed), 35 m s^{-1} (long-dashed) and a size radius of 300 km.

The disadvantage of this simple approach of specifying profiles is that a change in one structure parameter results in changes to several aspects of the structure. For instance, changing b in (6) changes the winds in both the inner and outer regions, and also the size, which makes it difficult to isolate which parameter contributes most to the resulting track (e.g., Chan and Williams 1987). Thus, a capability to modify the analytical profile is needed to vary the symmetric structure parameters independently.

The first modification procedure combines two profiles through a linear combination near a specified "match" point. Smoothing the combined profile using the Shuman (1957) procedure prior to the model initialization insures smooth variations of the derivatives. A second type of modification is to force a zero at some radius or at the midpoint of an interval in r. For example, the integrated relative angular momentum (RAM)

$$\text{RAM} \equiv \frac{\int_{r_1}^{r_2} r(rv)dr}{\int_{r_1}^{r_2} rdr}, \quad (8)$$

discussed by Willoughby (1988) may be changed from positive definite values for all profiles in Fig. 1 to a smaller (or even negative) value by forcing the profile to become negative at some radius. Details of these and other profile modification techniques are given in Fiorino (1987).

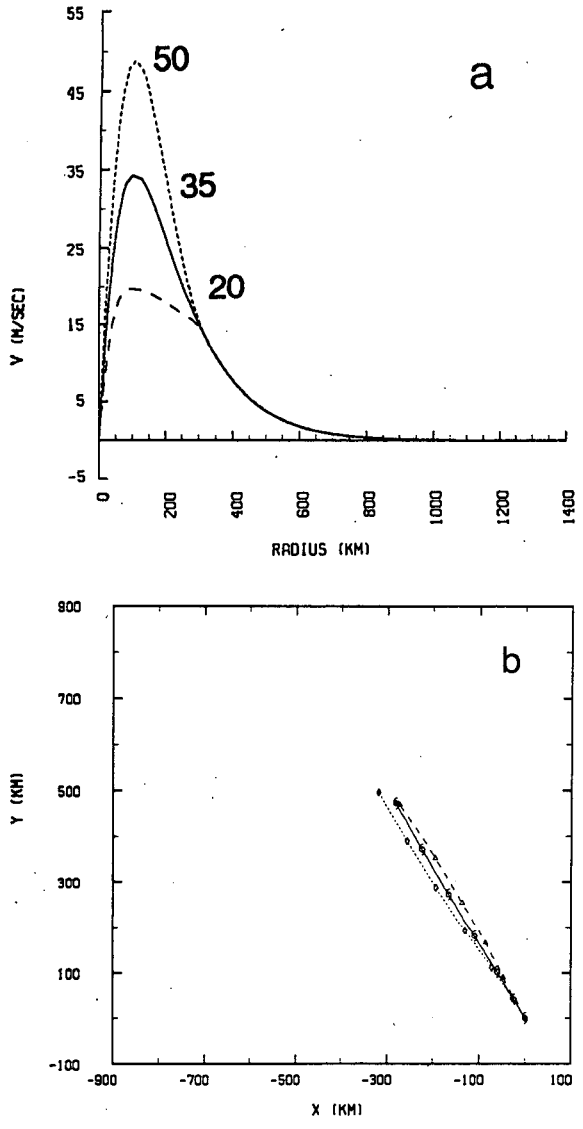

FIG. 2. (a) Tangential wind profiles with identical outer profiles and maximum intensity of 50 m s^{-1} (short-dashed), 35 m s^{-1} (solid) and 20 m s^{-1} (long-dashed) and (b) corresponding tracks to 72 h with the same line pattern as used in (a) and symbols along the tracks each 12 h.

a. Intensity effects

DeMaria (1985) suggested that cyclone intensity (maximum wind) had little effect on the motion in a nondivergent barotropic model. This can be demonstrated by imposing the initial tangential wind profiles in Fig. 2a. Notice that the profile beyond $r = 300$ km is fixed so that only winds in the inner region are varied according to the original profiles in Fig. 1. The corresponding tracks in the barotropic model with no basic current are shown in Fig. 2b. Only slightly greater northwestward displacements occur with the 50 m s^{-1} intensity vortex compared to the weaker storms. This clearly demonstrates that the inner region intensity has little effect on the motion of a storm in a nondivergent barotropic model.

A number of numerical sensitivity tests were carried out to determine if this result was dependent on resolution or domain size. Higher resolution (20 km) with the same domain size produced the same 72 h displacement of the vortex with $V_{max} = 35$ m s^{-1}. A lower resolution (80 km) model also produced only a slightly smaller displacement. It does not appear that resolution is a factor in the result of Fig. 2, so long as sufficient gridpoints are available to resolve the inner core region (diameter of 200 km). However, horizontal resolutions with less than six points within r_{max} did lead to small amplitude oscillations along the track. Reducing the domain size to 2000 km by 2000 km is unsatisfactory because the distortions due to the boundaries reduced the storm translation speed, even though the grid translated with the storm.

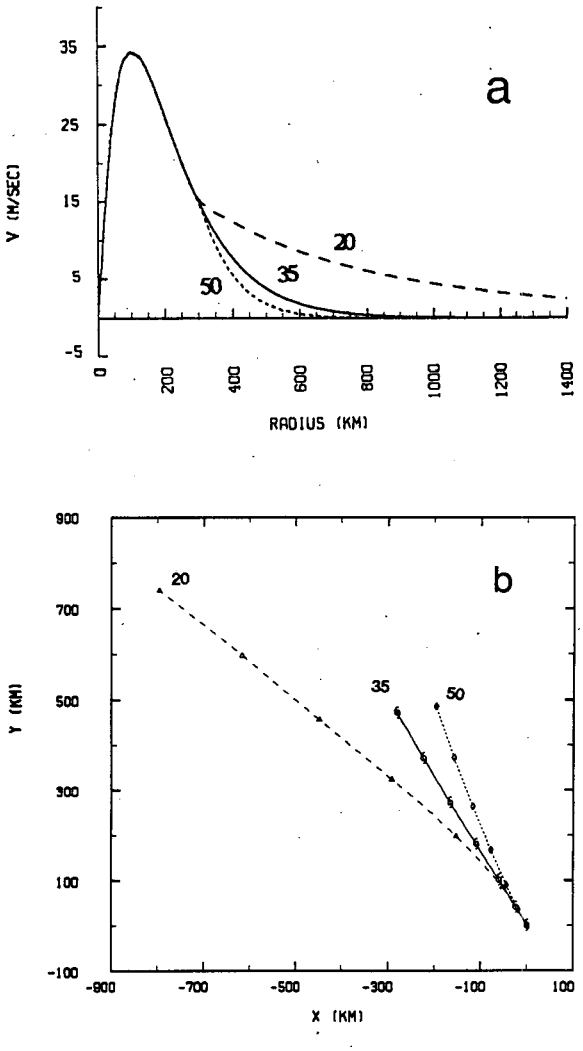

FIG. 3. As in Fig. 2, except for outer profiles corresponding to those in Fig. 1 and identical inner profiles.

b. Outer wind strength effects

The profiles in Fig. 3a are used to demonstrate the effect of the wind strength beyond 300 km. Notice that the wind profile inside 300 km is fixed (basic profile with a V_{max} = 35 m s^{-1} at r_{max} = 100 km). As shown in Fig. 3b, the motion of the vortex with stronger outer winds is much greater than the two other vortices that have small or zero winds at large radii. This result clearly indicates the importance of the strength of the flow outside 300 km on vortex translation. This region of the cyclone is not normally observed by aircraft reconnaissance because of the limited range of the aircraft and the operational requirements for fixing the location and intensity of the cyclone. This result suggests that the deviation of the storm track from steering (since this experiment includes no uniform flow) depends sensitively on outer regions of the storm that perhaps have not been specified well in operational analyses.

c. Symmetric perturbations

To better understand how the flow in this outer region influences track, the basic vortex (V_{max} = 35 m s^{-1} in Fig. 1) is perturbed in a cyclonic (positive v) and anticyclonic (negative v) sense (Fig. 4a). Such perturbations may occur in tropical cyclones, although the magnitude of changes may be difficult to observe over the data-sparse tropical oceans. The main purposes of these experiments are to demonstrate how the symmetric flow beyond r = 300 km would change the beta drift, and to indicate the importance of specifying the outer portion of the vortex in tropical cyclone prediction models and in future theoretical motion studies.

The corresponding 72-h tracks (Fig. 4b) indicate that these outer wind perturbations have caused turning motions in the same rotational sense as the flow changes in the r = 300–800 km annulus. For example, if the flow in the annulus is made more cyclonic, then the vortex track will turn cyclonically and move more toward the west in the Northern Hemisphere. The speed of motion also increases as the flow in this "critical" annulus increases in a cyclonic sense.

d. Translation speed as a function of outer wind strength

The above results suggest that the initial vortex flow beyond r = 300 km is an important factor in the beta drift. This dependency can be expressed in terms of the strength of the outer flow which is somewhat arbitrarily defined by

$$V_{s0} = \left\{ \frac{\int_{300\text{ km}}^{1000\text{ km}} rv^2\,dr}{\int_{300\text{ km}}^{1000\text{ km}} r\,dr} \right\}^{1/2}. \qquad (9)$$

The velocity in the numerator is squared since the tangential wind can change sign in this region. An upper limit of 1000 km (versus the 800 km discussed above) is specified to allow for larger vortices.

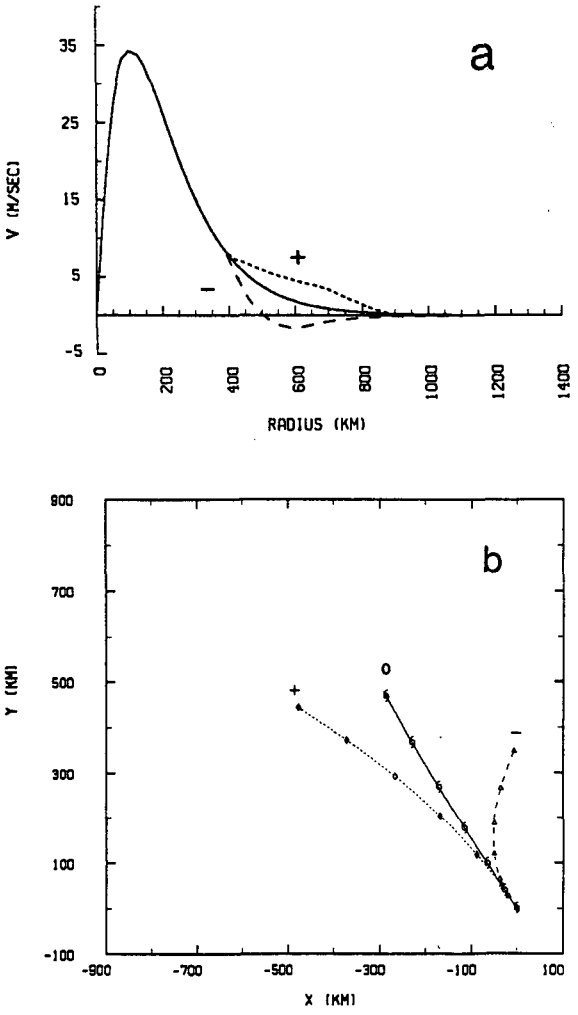

FIG. 4. As in Fig. 2, except for cyclonic (short-dashed) and anticyclonic (long-dashed) perturbations added to the basic symmetric vortex (solid) in the 300–800 km annulus.

The relationship between the vortex translation speed (relative to the steering that is not included here) and the outer strength is shown in Fig. 5 for the various initial wind profiles tested (see list in Fiorino 1987). Although the speed of motion is generally proportional to the initial outer strength of the vortex, the relationship is not perfect, especially for smaller values of outer wind strength.

In summary, the above sensitivity tests for different initial conditions demonstrate that the flow in the r = 300–800 km annulus is related to the direction and speed of beta drift. The translation speed (relative to the steering flow) during the slowly varying state in these model simulations is nearly proportional to initial outer strength. In addition, the direction of motion is influenced by the magnitude and the sense (i.e., cy-

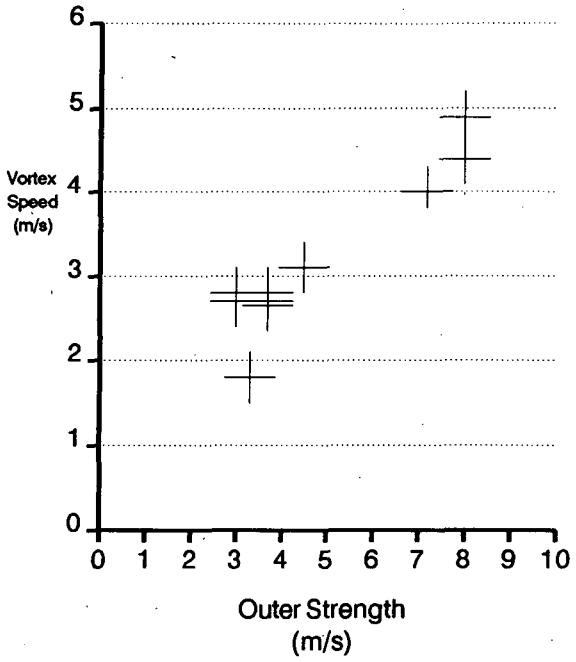

FIG. 5. Speed of motion (m s^{-1}) during the slowly-varying state versus outer wind strength (m s^{-1}) for all initial-vortex sensitivity experiments.

clonic or anticyclonic) of the tangential flow. Thus, apparently subtle changes in the outer vortex structure may lead to significant track deviations, whereas inner region features such as V_{max} and r_{max} have little effect. The applicability of these results to more realistic tropical cyclone track forecast models is limited to the degree that these barotropic motion processes dominate other effects in the more complete models.

These experiments also suggest that initializing the vortex in a numerical model by specifying only a size radius may be insufficient. In these experiments with a fixed radius of 15 m s^{-1} winds, the flow in the 300–800 km annulus appears to be controlling beta drift. Evidently, the vortex flow beyond the size radius should also be carefully specified. This implies that it will be necessary to measure the vortex flow beyond $r = 300$ km (perhaps out to $r = 1000$ km). Such measurements would have to be fairly accurate as changes on the order of 1–3 m s^{-1} have a significant effect on the track, particularly with regard to direction of motion.

4. Symmetric and asymmetric circulations

A planning group reviewing the theory of tropical cyclone motion (Elsberry 1986) recommended that the total flow system be divided into three components:

(i) An axially symmetric circulation representing the vortex;

(ii) An asymmetric circulation that arises from an interaction between the symmetric circulation and the "environment" (the earth's vorticity field and larger-scale flows);

(iii) A larger-scale "steering" flow that represents horizontally uniform steering effects.

As indicated above, the possible ambiguity between any asymmetric components of the steering flow and that associated with the interaction is eliminated in this model by the initial no-flow environment. That is, the model is started from an initially symmetric, isolated vortex on a β plane. In this situation, the asymmetric flow is only due to interaction of the vortex with the earth's vorticity field (the Coriolis parameter).

a. Calculation procedures

The first step in the symmetric/asymmetric separation is to interpolate the solution to a cylindrical grid centered on the storm (point of minimum ψ). To locate the center, the point of zero gradient in ψ is linearly interpolated between local derivatives of ψ to the east (north) and west (south) of the grid point with the minimum ψ. The cylindrical grid has a radial increment of 20 km and an azimuthal (θ) increment of eight degrees (45 sectors). The interpolation from the model grid to the cylindrical grid is performed with a bicubic spline routine from the National Center for Atmospheric Research (NCAR) Scientific Subroutine Package (SSP) using the same boundary conditions as in the model.

The symmetric component of the field on the cylindrical grid is found by averaging along θ at each radius, which generates a function tabulated at uniform points in r. The symmetric component at each model grid point (x, y) is specified by interpolating from the symmetric component [e.g., $\psi_s(r)$] using a spline under tension (NCAR SSP). The asymmetric component on the model grid is then found by subtracting the symmetric component from the total [i.e., $\psi_a(x, y)$fj= $\psi_t(x, y) - \psi_s(x, y)$]. The symmetric and asymmetric components in the corners of the x, y grid with radii greater than the cylindrical grid are set to the value of the function at the outer edge of the cylindrical grid. Tests with symmetric/asymmetrical analytical functions specified on the model grid demonstrated that the procedure was able to very accurately recover the true symmetric/asymmetric components.

The symmetric/asymmetric flow calculation procedure is applied only to the ψ_t solution. All other quantities (e.g., ζ_a from ψ_a) are then derived using diagnostic relationships based on the model finite differences to ensure maximum consistancy with the model solutions.

b. Symmetric vortex evolution

The evolution of the tangential wind profiles to 144 h is given in Fig. 6 for the basic vortex (V_{max} = 35 m s^{-1} in Fig. 1) and the weak-large vortex (V_{max} = 20 m s^{-1} in Fig. 1). Although the maximum wind speed is

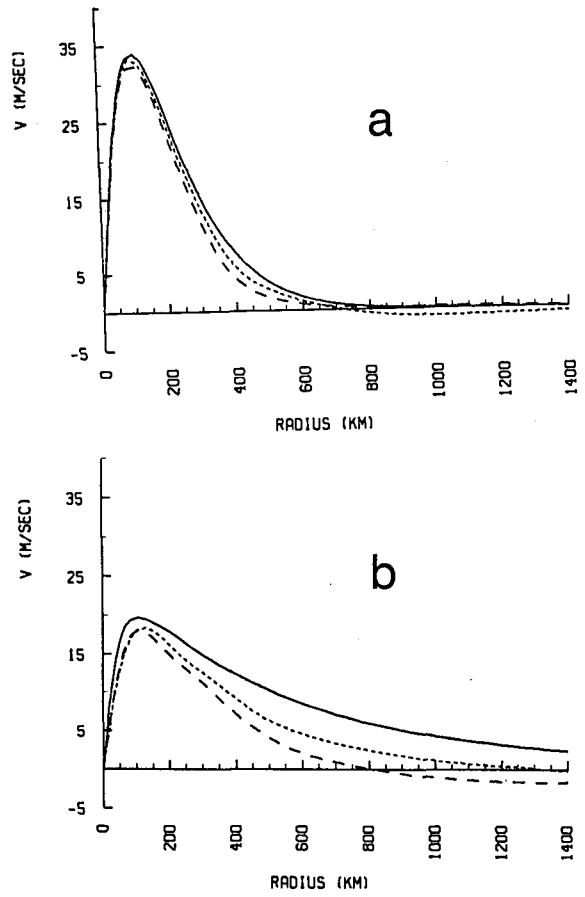

FIG. 6. Evolution of the tangential wind profile at $t = 0$ (solid), 72 h (short-dashed), 144 h (long-dashed) for (a) the basic vortex and (b) the weak-large vortex.

nearly maintained, large decreases in cyclonic circulation occur at large radii. This is especially true for the weak-large vortex (Fig. 6b), since anticyclonic flow has formed beyond $r = 700$ km at $t = 144$ h. Whereas the initial RAM between the center and 1600 km calculated from (8) was 70 (10^{18}) m^2 s, the RAM values decrease steadily to a minimum at about 100 h. After 100 h, the RAM values oscillate about small negative value. At 144 h the RAM is -25 (10^{18}) m^2 s. Other initial vortices tested also experienced a decrease in magnitude of RAM with time, as is implied from the profiles in Fig. 6. This is consistent with Tojo (1953) who calculated the tangential wind profile for a moving vortex and demonstrated the formation of an outer anticyclone and negative RAM as a consequence of conservation of absolute vorticity.

c. *Asymmetric circulation evolution*

A time sequence of the asymmetric streamfunction (ψ_a) for the basic vortex experiment is given in Fig. 7. The general features of the asymmetric streamfunction are: (i) a dipole-like pattern with an anticyclonic gyre to the east of the center and a cyclonic gyre to the west; (ii) a "ventilation" flow between the anticyclonic and cyclonic gyres; (iii) a "buckle" at the center where ψ_a and the gradient of ψ_a go to zero, which defines a small region around which the asymmetric wind appears to flow; and (iv) a cyclonic twisting or rotation of the gyre centers that reorients the ventilation flow from northward at the initial time to northwestward at later times. These four features are highlighted in Fig. 7a.

The amplitude of the large-scale asymmetric gyres, which are referred to as "beta gyres" since they are associated with the beta term, increases with time (Fig. 8a). Three stages in the beta gyre development from an initially symmetric vortex are apparent. During the first 12 h of the integration, rapid growth of the gyres quickly establish the circulation (rapid growth phase). From 12 to 48 h, the gyre amplitude grows almost linearly (linear growth stage) and a steady-state phase occurs from 48 to 72 h. The translation speed of the vortex (Fig. 8b) follows a similar evolution as the magnitude of ψ_a, which suggest that the ventilation flow between the beta gyres is directly related to the translation speed. In contrast to the time scale for the evolution of the translation speed, the direction of motion stabilizes to within 5° of the steady-state value of 320° within 3 h. This finding is similar to DeMaria (1985), except that the direction of motion in this experiment is less variable in time.

These changes in Fig. 8 are useful in understanding the temporal variations of ψ_a in Fig. 7. At $t = 6$ h (Fig. 7a), the gyre centers are approximately 450 km from the cyclone center and have already shifted to orient the ventilation flow toward about 320°, which is similar to the storm motion vector. Since the area of perturbed asymmetric flow is confined to a domain of approximately $r = 300$ km, the contours farther away from the perturbed zone are still aligned north to south. If all of the gyre circulation was aligned east–west, this pattern would be analogous to the pattern of vorticity tendencies based on linear (βv) reasoning (Anthes and Hoke 1975; Holland 1983). However, the nonlinear advective effects have already produced a cyclonic rotation of the beta gyre flow within about 300 km of the center after only 6 h.

During the rapid growth phase (Fig. 8a), the gyres build in intensity and expand outward. Similarly, the region of rotated flow expands outward and results in a broader ventilation flow. This ventilation flow continues to increase at $t = 24$ h (Fig. 7c) during the linear growth phase, and the ψ_a field farther from the cyclone center becomes distorted in the east–west direction. At $t = 72$ h, (Fig. 7d), the anticyclonic gyre to the east has rotated clockwise, although the center of this gyre appears to be lagging behind the moving center. Nevertheless, the ventilation flow in the inner region maintains the same intensity and horizontal extent. Even though the amplitude of the asymmetric circulation

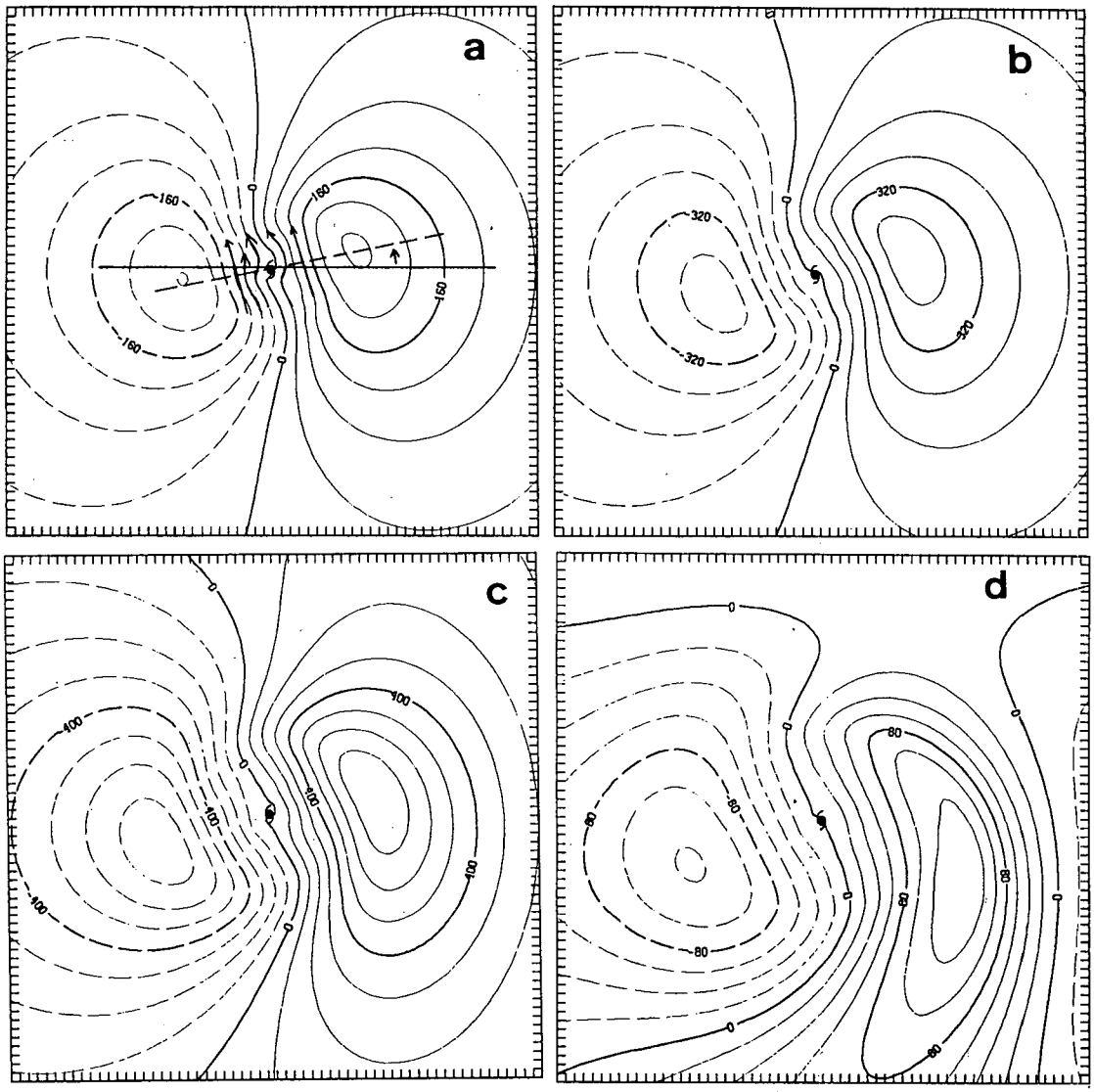

FIG. 7. Temporal evolution of the asymmetric streamfunction ψ_a ($m^2 s^{-1}$) at (a) 6 h; (b) 12 h; (c) 24 h; and (d) 72 h. The plot domain is 61 × 61 points (with Δx = 40 km, 2400 × 2400 km) centered on the vortex. The tick marks indicate the location of the grid points. This domain size is used in all subsequent figures unless otherwise noted. Positive (negative) values indicate anticyclonic (cyclonic) streamfunctions. Contour intervals are 4, 8, 10 and 20 (10^4), and the maximum absolute values of ψ_a are 2.5, 4, 7 and 12 (10^5), respectively.

has reached a steady state (Fig. 8a), the development of east–west distortions suggests the formation of an azimuthal wavenumber two asymmetry. An alternate explanation is that the basic wavenumber one circulation is breaking down in the very weak flow in the outer portions ($r > 700$ km) of the system.

Longer integrations to $t = 144$ h (not shown) indicate that the breakdown in the asymmetric flow at large radii continues, although the track remains essentially steady from t = 72–144 h. The "trailing lobe" of the anticyclonic gyre at t = 72 h (Fig. 7d) splits into a separate circulation feature and then rotates anticyclonically and results in a new anticyclonic center east of the center. During this bifurcation, the ventilation flow between the gyres and the vortex translation speed remain approximately steady.

The fact that the vortex motion continues even with significant changes in the outer asymmetric flow implies that the critical motion dynamics are occurring within the region of "significant" symmetric flow. A measure of the significant symmetric flow is the horizontal scale of the gyres at t = 72 h, which is approximately r = 700 km. This scale coincides with the point at which the symmetric component of vortex reverses from cyclonic to anticyclonic circulation (see Fig. 6a) at t = 72 h. The implication is that a quasi-steady state

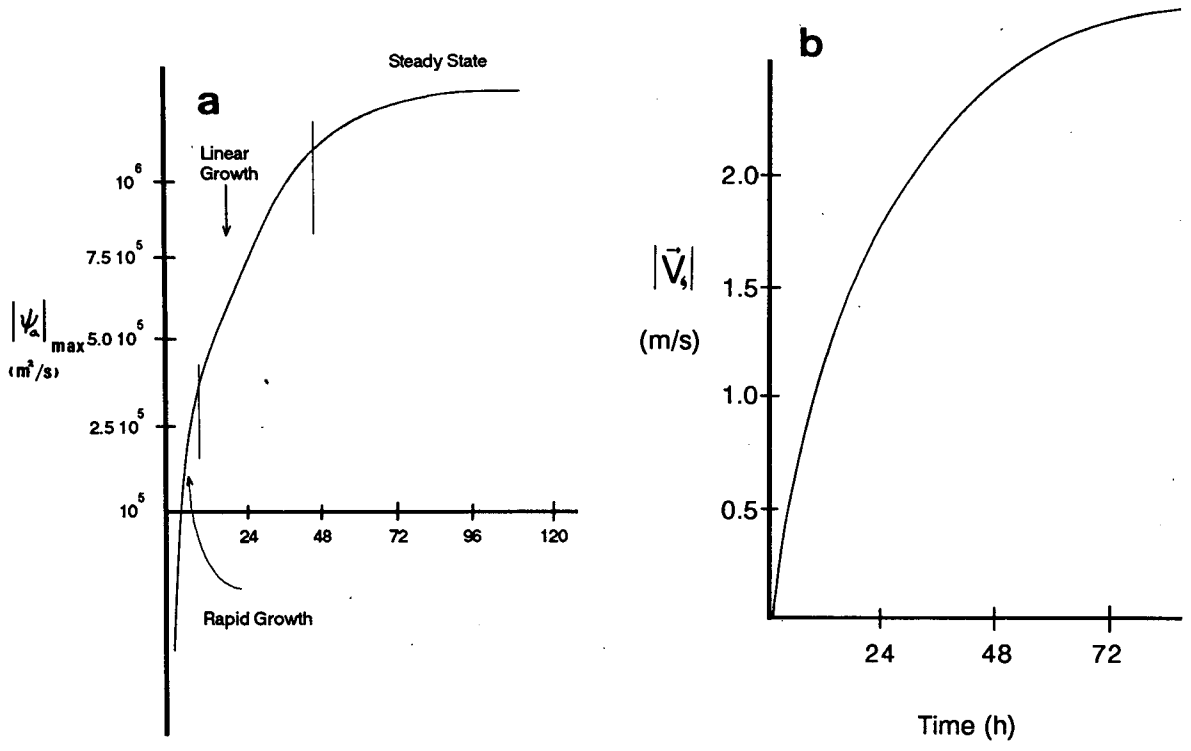

FIG. 8. Time variation of (a) the maximum amplitude of the ψ_a gyres of the basic vortex experiment and (b) the corresponding translation speed for the center.

between linear forcing and nonlinear vorticity advection is achieved within this region.

To more explicitly relate the motion of the vortex to the asymmetric circulation, the asymmetric flow is derived from ψ_a via

$$u_a = -\frac{\partial \psi_a}{\partial y}, \quad v_a = \frac{\partial \psi_a}{\partial x}. \tag{10}$$

The asymmetric flow at $t = 72$ h for the basic vortex is shown in Fig. 9 from a large-scale and a small-scale view. A strong relationship is evident between the asymmetric flow in the vicinity of the center and the vortex motion vector. This relationship is better illustrated by removing an average motion vector between $t = 66$ h and $t = 78$ h from the asymmetric flow to form the "relative" asymmetric flow (Fig. 10). Over most of the symmetric vortex circulation region, the asymmetric flow is nearly equal to the average motion vector and the relative flow is very small. However, smaller gyres (about 100 km) with relative wind speeds up to 5 m s^{-1} are found in the inner core region. When the asymmetric circulation is defined relative to the streamfunction minimum, the storm appears to be translating faster than the asymmetric flow in the inner region. Consequently, a flow from ahead to behind the storm center arises because of the definition of the coordinate system. Similar inner region gyres have been observed by Marks and Houze (1987) in Hurricane Norbert in the eastern North Pacific.

The inner gyres in this model vary depending on the definition of the coordinate system. If the origin of the coordinate system is defined at the maximum vorticity center, these inner gyres are reversed as the storm is then translating slower than the asymmetric flow in the inner region. If the origin of the coordinate system is placed halfway between the maximum vorticity and the streamfunction center, the inner gyres essentially disappear. Because of the arbitrariness in these definitions of the coordinate systems, it seems likely that these inner gyres have little real impact on the motion of the vortex in the model.

A "ventilation flow vector" is defined as the average asymmetric flow within $r = 300$ km of the streamfunction center for comparison with the motion vector of the center (Fig. 11). This averaging area for the ventilation flow vector is chosen based on the size of the cyclonic vortex ($r \sim 300$–500 km) and the best fit to the center motion vector. The translation speed is calculated over 12-h increments centered on 12, 24, 36 ... 132 h based on hourly positions of the streamfunction minimum. These hourly positions are smoothed prior to the translation speed calculation to remove numerically-generated position and speed oscillations.

As noted earlier in Fig. 8b, the motion rapidly builds, and then grows linearly in time until a maximum is reached around $t = 60$ h. After the maximum translation speed has been achieved, the speed of motion

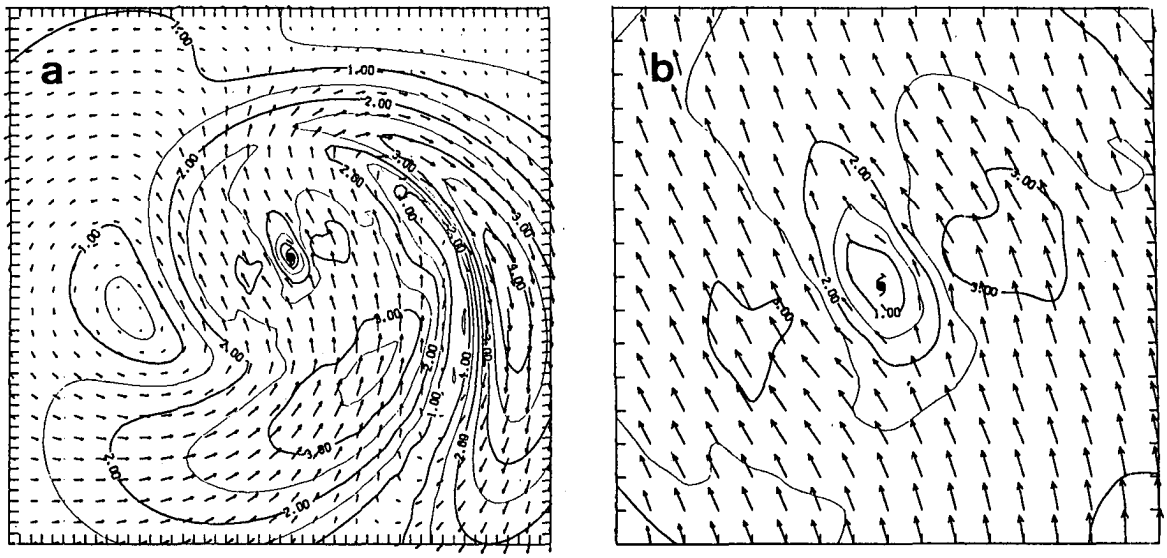

FIG. 9. Asymmetric flow at t = 72 h for the basic vortex within a domain of (a) 2000 × 2000 km and (b) 640 × 640 km region. The flow speed (m s^{-1}) is contoured with an interval of 0.5 m s^{-1} in both panels. The maximum vector length corresponding to two grid points (between two tick marks) is 5 m s^{-1}.

slowly oscillates about some quasi-steady value. The magnitude of the ventilation flow vector follows the motion in a nearly lock-step manner, but is about 5–10% smaller (slower) than the actual vortex motion in the steady state. This small deviation is only weakly dependent on the storm center definition and on the existence of the weak winds within 100 km radius. The corresponding directions of motion are given in Fig. 11b. The greatest departures occur during the rapid growth phase of the beta gyres. During the slowly varying stage, the vortex is moving consistently about 5° to the left of the ventilation flow.

The composite studies of Chan and Gray (1982) and the geostrophic steering-flow analysis of Brand et al. (1981) showed that tropical cyclones tend to move to the left of some averaged "large-scale" environmental flow vector. In these observational studies, the cyclones tended to move faster than the basic flow vector. Since the results in Fig. 8 do not fit the observed relationship precisely, further studies of the observed difference vectors are necessary.

5. Streamfunction tendency analysis

The development of the asymmetric gyres in relation to the initial vortex structure is best interpreted in terms of the model tendency equation for the total streamfunction (ψ_t),

$$\frac{\partial \psi_t}{\partial t} = H^{-1}\{-J(\psi_t, \nabla^2\psi_t)\} + H^{-1}\{(\beta v)\} \quad (11)$$

where H^{-1} is the inverse operator of $H(f) = \nabla^2 f$. Splitting the nonlinear advection and beta terms into asymmetric (A) and symmetric (S) components yields,

$$\frac{\partial \psi_t}{\partial t} = H^{-1}\{-J(\psi_a, \nabla^2\psi_s)\} + H^{-1}\{-J(\psi_s, \nabla^2\psi_a)\}$$

TT ASVA AAVS

$$+ H^{-1}\{S(\beta v)\} + H^{-1}\{A(\beta v)\}, \quad (12)$$

SB AB

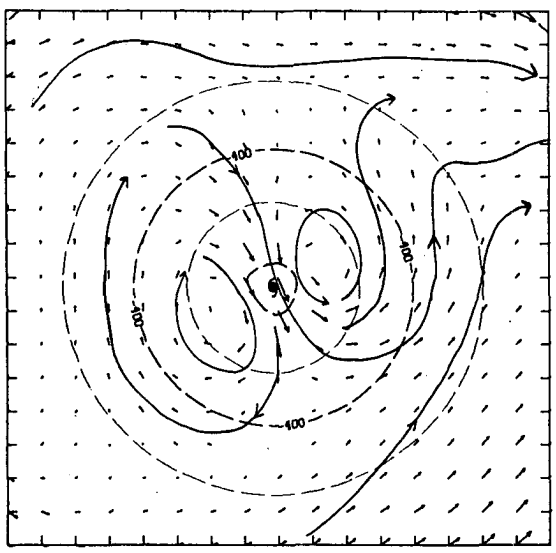

FIG. 10. As in Fig. 9b, except for relative asymmetric flow (arrows) formed by subtracting the motion vector at 72 h. The maximum arrow length in the upper right corner corresponds to 5.0 m s^{-1}. The symmetric streamfunction (dashed contour interval of 200 (×10^5) m^2 s^{-1}) depicts the scale of the symmetric vortex circulation.

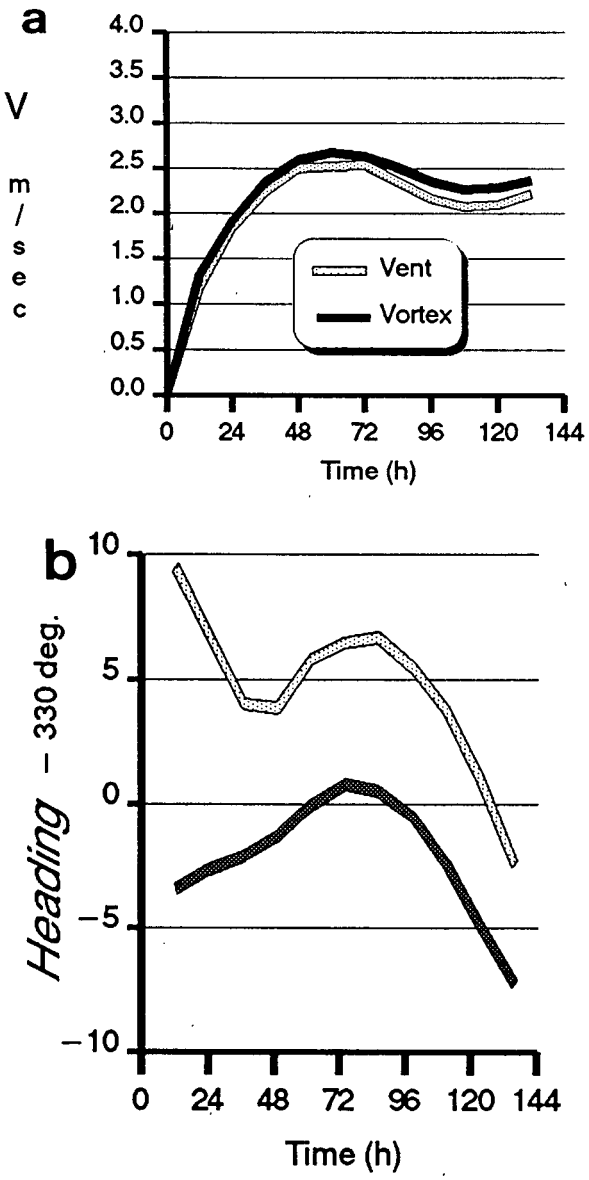

FIG. 11. (a) Magnitude and (b) direction relative to 330° of the ventilation flow vector (open line) compared to the speed and direction of vortex motion (solid) for the basic vortex.

where

TT	Total tendency
ASVA	Advection of symmetric vorticity by the asymmetric flow
AAVS	Advection of asymmetric vorticity by the symmetric flow
SB	Symmetric component of the beta term that forces the asymmetric flow
AB	Asymmetric component of the beta term that forces the symmetric flow

These tendencies are calculated on the model grid using the model finite difference operators based on the ψ_s, ψ_a fields. The nonlinear term involving the advection of asymmetric vorticity by the asymmetric streamfunction is omitted in (12) because it is an order of magnitude less than ASVA or AAVS. The linear operators S and A return the symmetric and asymmetric components of the beta term SB and AB, respectively. To understand how the total tendency field arises, the contributions of the nonlinear and linear terms are examined separately.

a. Linear effects

The beta term produces a large-scale, dipole-type tendency field (Fig. 12) with a significant magnitude that always is oriented east-west relative to the (moving) storm center. The maximum/minimum points at all times occur at about $r = 250$ km. Comparison with the asymmetric streamfunction fields in Fig. 7 indicates that the beta term is the primary source for the asymmetric flow, which is the justification for the beta gyre terminology.

During the rapid growth phase (Fig. 12a, b), the zero line in the beta tendency is aligned nearly north–south, which indicates a forcing that is symmetric in the east–west direction. However, an east–west distortion occurs during the linear growth and steady-state phases (Fig. 12c, d). Outside of $r = 500$ km, the positive zone is wrapped around the inner part of the vortex. By $t = 72$ h, the region of the cyclonic tendencies to the west of the center has decreased in area and a new region of cyclonic tendencies has emerged on the far eastern side of the system. This distortion is due to the asymmetric circulation that has formed, but there is still an essentially east–west symmetry in the pattern. Notice specifically that the beta term can not be directly responsible for the rotation of the large-scale asymmetric gyres in Fig. 7 because this forcing is aligned east–west.

At the initial time when the vortex is symmetric, an azimuthal average of βv would go to zero. However, the βv term later can have a contribution to the symmetric component of ψ because of the development of stronger meridional components east of the storm center (Chan and Williams 1987). The symmetric component of the β term (Fig. 13) at $t = 6$ h contributes to only slight ψ rises within 100 km of the center. These positive values over the center represent an anticyclonic tendency that weakens the symmetric low. By 72 h, the area of ψ rises has shrunk and an area of falling ψ occurs beyond $r = 800$ km. It appears that the evolution of the symmetric circulation is primarily determined by the beta term, and this accounts for the slow weakening of the tangential wind near the center of the vortex in Fig. 6.

The beta tendency pattern also indicates indirectly the formation of a southerly flow ($\beta v > 0$) over the center. This flow must reach a maximum in the inner region for the symmetric beta term to peak at the cen-

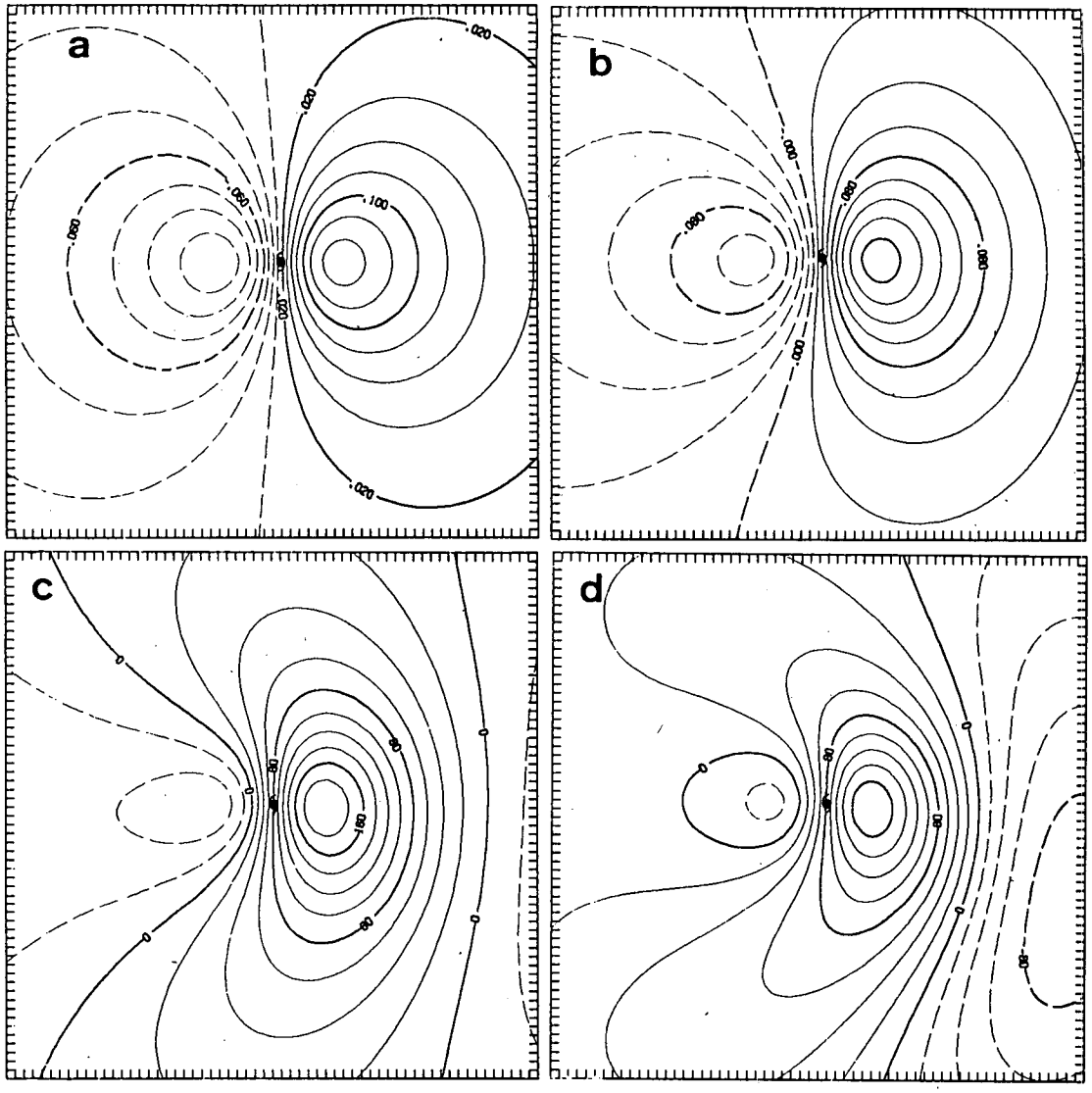

FIG. 12. Total streamfunction tendency due to the linear (βv) term at (a) 3 h, (b) 12 h, (c) 36 h, and (d) 72 h. Positive (solid) and negative (dashed) ψ_a tendencies correspond to increasing anticyclone and cyclonic circulations respectively. Contour interval is 0.02 in (a) and (b) and 20 ($\times 10^{-3}$) in (c) and (d) and the maximum absolute values are 0.14, 0.16, 0.18 and 0.16, respectively.

ter. Thus, the northward component (southerly ventilation flow) of the motion is indirectly related to the slight filling of the inner vortex low. Notice also that the β tendency in Fig. 13b indicates the development of a *cyclone* beyond $r = 700$ km whereas the tangential wind profile shows *anticyclonic* flow. Thus, development of the outer anticyclone must be related to the *asymmetric* component of the βv tendency.

The asymmetric component of the beta term (Fig. 14) accounts for most of the total beta tendency. This asymmetric component is clearly related to the formation of the asymmetric gyres, as evidenced by the large scales and the greater magnitude of the forcing away from the inner regions of the symmetric vortex. The anticyclonic forcing east of the center contracts in time. By $t = 72$ h (Fig. 14b), a second cyclonic forcing center has developed farther to the east, which is associated with the development of anticyclonic flow in Fig. 6. Notice also the azimuthal wavenumber two features around $r = 700$ km (near the boundaries of the domain shown). An important observation from Fig. 14 is that the amplitude and distribution of the asymmetric β forcing is also asymmetric. Notice the greater areal extent and greater intensity of the cyclonic (<0) tendencies compared to the anticyclonic tendencies (>0) in Fig. 14. As noted above, the asymmetrical distribution of v also causes a net change in the symmetric streamfunction $\psi(r)$ that leads to an anticyclonic tendency in the outer region tangential flow.

The Rossby dispersion process, associated with the

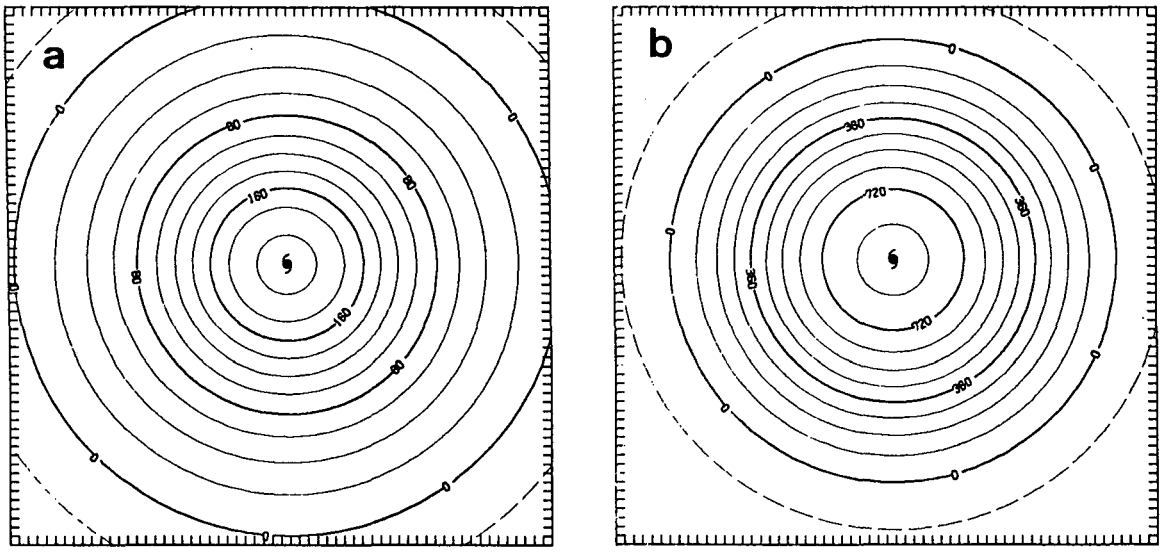

FIG. 13. Symmetric component of the β term at (a) 6 h and (b) 72 h. Positive ψ_s tendencies indicate increasing anticyclonic (decreasing cyclonic) circulation with time. Contour intervals are 20 ($\times 10^{-4}$) and 90 ($\times 10^{-4}$), and the maximum absolute values are 0.02 and 0.09, respectively.

linear beta term, is strongly linked to the formation of the asymmetric circulation and to the outer wavenumber two features. However, the basis of this forcing is the v component of the vortex flow that is strongly influenced by nonlinear advective effects. Thus, the nonlinear term must be examined to understand how the linear forcing is modulated through symmetric/asymmetric interaction and the motion process.

b. *Nonlinear effects*

The advection of the symmetric circulation by the asymmetric flow (ASVA) is portrayed in Fig. 15. A motion-type dipole pattern of negative ψ tendencies (cyclonic) to the northwest and positive ψ tendencies (anticyclonic) to the southeast is clearly evident. The orientation of these dipoles was more north–south at t = 3 h and 6 h (not shown). The horizontal scale of this advection pattern is essentially constant throughout the integration. This dipole pattern shows again that the vortex on the scale of r = 300–400 km is being translated by the asymmetric circulation associated with the large-scale beta gyres.

The advection of the asymmetric circulation by the symmetric vortex (AAVS) is shown in Fig. 16. The

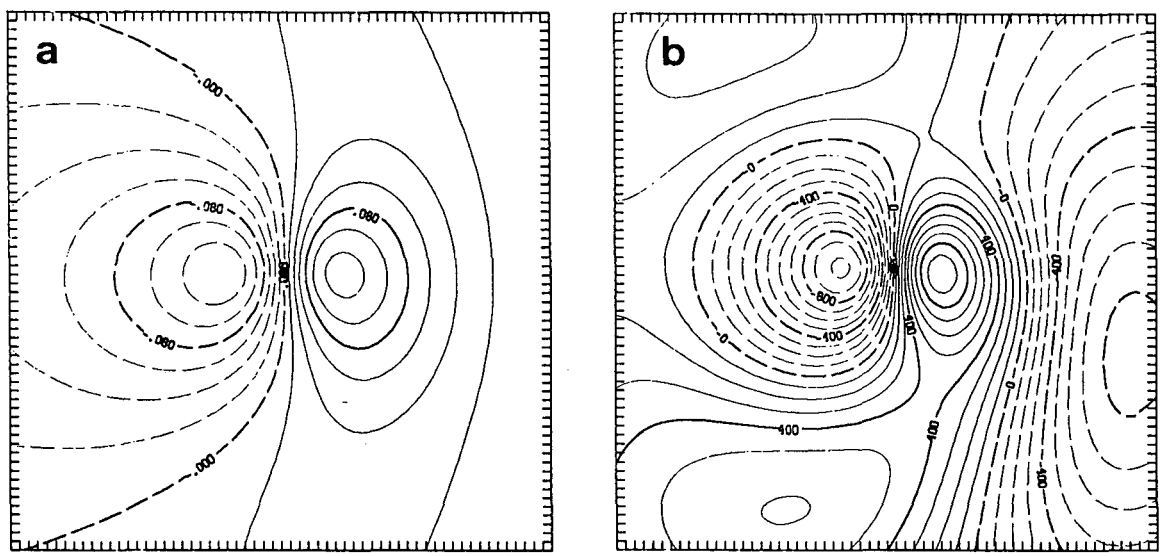

FIG. 14. Asymmetric component of the β term at (a) 24 h and (b) 72 h. Positive (solid) and negative (dashed) ψ_a tendencies correspond to increasing anticyclone and cyclonic circulations. Contour intervals are 0.02 and 100 ($\times 10^{-4}$), and the maximum absolute values are 0.12 and 0.10 respectively.

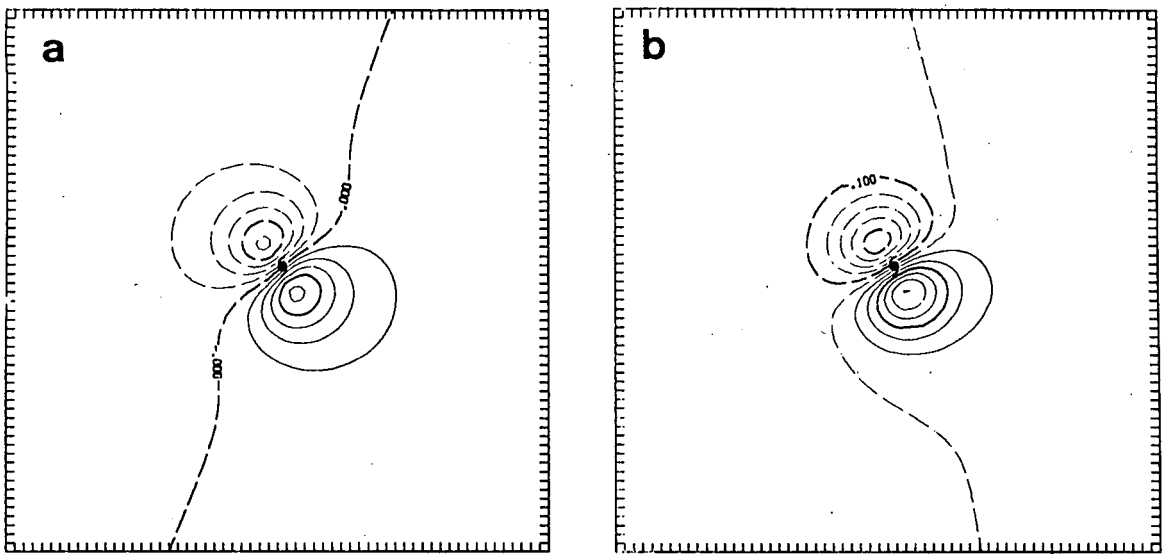

FIG. 15. Contribution to the streamfunction tendency due to advection of symmetric vorticity by the asymmetric flow at (a) 12 h and (b) 72 h. Positive (solid) and negative (dashed) ψ_a tendencies correspond to increasing anticyclone and cyclonic circulations respectively. Contour intervals are 0.1 and 0.06 and the maximum absolute values are 0.3 and 0.10 respectively.

asymmetric flow has been heavily smoothed in the inner regions (e.g., see Figs. 7 and 9) prior to the calculation of the tendency to emphasize this advective effect in the outer portions of the vortex. A large-scale dipole pattern of positive tendencies (anticyclonic) to the northwest and negative tendencies (cyclonic) to the southeast is present at 6 h (Fig. 16a). This pattern arises as the symmetric circulation tends to rotate the asymmetric gyres that are being produced by the linear beta term (Fig. 12). Distortion of the asymmetric circulation then causes a further rotation of the AAVS dipole at 12 h (Fig. 16b) and at 24 h (Fig. 16c). By t = 72 h (Fig. 16d), the forcing is roughly 180° out of phase with the beta gyres and nearly counteracts gyre development due to linear (βv) forcing (Fig. 12d). Also note how the gyre rotation effect (e.g., positive tendencies to the north of the center) is first achieved near the center by the higher winds in that region, and then expands outward in time. Although the rotation of the asymmetric beta gyres occurs at all radii initially, the steady state is approached at different times depending on the strength of the vortex circulation.

It is important to stress the role of nonlinear effects in orienting the ventilation flow. Previous theories (e.g., Adem 1956; Holland 1983) associate the westward component of beta drift with Rossby dispersion alone. This was shown to be incorrect by Chan and Williams (1987), who demonstrated that the linear term alone (Rossby dispersion) only moved the center slightly. The results presented here have more precisely illustrated how the nonlinear term induces the motion, and more significantly how advection of the asymmetric circulation by the symmetric flow modifies the direction of motion. Thus, the westward component of beta drift in the model arises strictly from advective process and is only indirectly related to linear effects.

6. Summary of the dynamics of beta drift

The development and evolution of the symmetric and asymmetric circulations in a tropical cyclone vortex moving on a β plane has been studied within the context of a nondivergent barotropic model. A procedure has been developed to uniquely and accurately decompose the streamfunction field on a Cartesian grid into azimuthally symmetric and asymmetric components on the input grid (given the ψ center position). This decomposition has been applied only to the model solution. All other quantities (e.g., vorticity and wind) have been diagnosed to interpret more precisely the model solution. An experiment with a typical vortex profile has been analyzed in detail using this procedure to illustrate how vortex structure influences the motion. Experiments with other vortices confirm the role that vortex structure can have in causing deviations from a steering flow concept.

The symmetric flow, as represented by the tangential wind profile, experiences a slight weakening of the maximum wind speed and the formation of an anticyclone beyond r = 600 km. It is generally observed that the various initial vortices evolve toward a common tangential wind profile in this nondivergent barotropic model. The integrated relative angular momentum (RAM) in the r = 0–2000 km annulus generally decreases and then undergoes oscillations during a 144 h integration.

The asymmetric circulation has an azimuthal wavenumber one appearance with an anticyclone east of

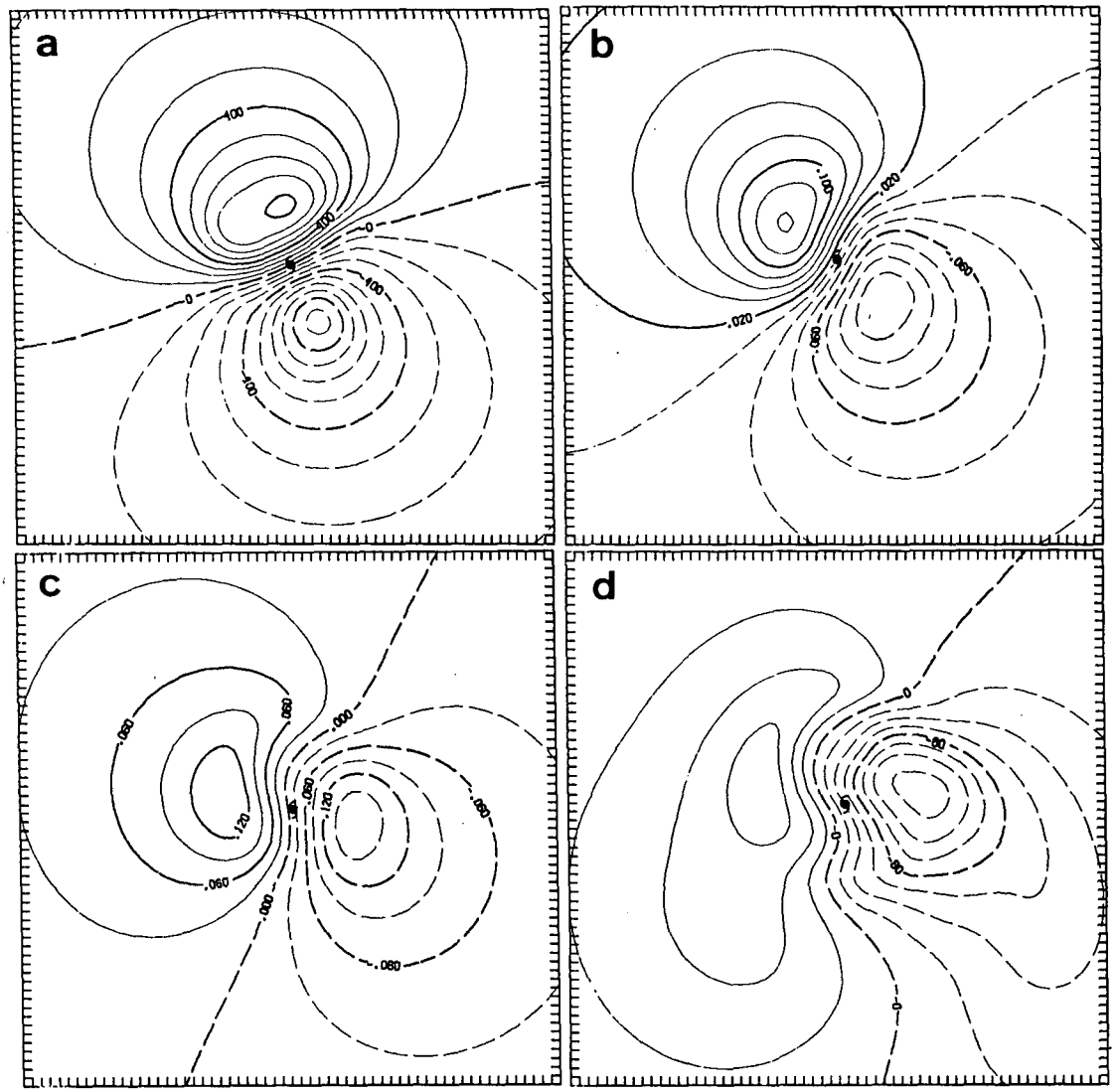

FIG. 16. Contribution to the streamfunction tendency due to advection of asymmetric vorticity by the symmetric flow (AAVS) at (a) 6 h, (b) 12 h, (c) 24 h and (d) 72 h. Positive (solid) and negative (dashed) ψ_a tendencies correspond to increasing anticyclone and cyclonic circulations respectively. Contour intervals are 100 ($\times 10^{-4}$), 0.02, 0.03 and 20 ($\times 10^{-3}$), respectively and the maximum absolute values are 0.08, 0.14, 0.15 and 0.14 respectively.

the center, a cyclone to the west and a nearly uniform, broad-scale ($r \sim 300$ km) ventilation flow between the gyres. The ventilation flow is almost exactly equal to the storm motion vector over the entire area of significant symmetric streamfunction. The only exception occurs in the inner core (within the radius of maximum wind). In this inner core, the winds go to zero, which results in a small dipole in the relative asymmetric flow with an orientation opposite to that of the larger scale asymmetric gyres. However, these inner gyres essentially disappear if the origin of the asymmetric circulation calculation is placed halfway between the minimum streamfunction and maximum vorticity centers.

The dynamical issues are to explain the formation of the large-scale gyres, why they rotate to orient the ventilation flow towards the northwest, and why the gyres reach a steady state. Analysis of the model streamfunction tendency equation demonstrates that the linear β term is responsible for the initial formation of the asymmetric "beta" gyres. Nonlinear advective processes have two roles. The first is the advection of the symmetric vortex (especially in the inner 400 km) by the ventilation flow between the asymmetric gyres. This component of the nonlinear term has the greatest magnitude. The second role of the nonlinear advection is to balance the linear β forcing through a rotation of the asymmetric circulation by the symmetric vortex flow and to orient the ventilation flow toward the northwest (Northern Hemisphere). That is, the nonlinear processes act to maintain the asymmetric flow

in a steady state against constant linear forcing and are responsible for the westward component of beta drift through a rotation of the ventilation flow between the beta gyres. In conclusion, the motion of a tropical cyclone-scale vortex in a nondivergent barotropic model can be viewed as a set of symmetric/asymmetric circulation subsystems that move and sustain each other in a quasi-balanced manner.

Acknowledgments. This study is a portion of the dissertation research of M. Fiorino under the direction of R. L. Elsberry, whose participation was partially funded by the Office of Naval Research (Marine Meteorology Program). The lead author acknowledges the generous support of Fleet Numerical Oceanography Center for computational and other resources and of his former employer (Naval Environmental Prediction Research Facility) who provided funding for his Ph.D. program and continued to provide assistance during the research. Members of the Ph.D. committee (R. T. Williams, C.-P. Chang, R. H. Franke and P. A. Jacobs) are thanked for their contributions. G. J. Holland provided comments on the manuscript, which was skillfully prepared by Mrs. Penny Jones.

REFERENCES

Adem, J. 1956: A series solution for the barotropic vorticity equation and its application in the study of atmospheric vortices. *Tellus*, **8**, 364–372.

Anthes, R. A., and J. Hoke, 1975: The effect of horizontal divergence and the latitudinal variation of the coriolis parameter on the drift of a model hurricane. *Mon. Wea. Rev.*, **103**, 757–763.

Arakawa, A., 1966: Computational design for long-term numerical integrations for the equations of atmospheric motion. *J. Comput. Phys.*, **1**, 119–143.

Brand, S., C. A. Buenafe and H. D. Hamilton, 1981: Comparison of tropical cyclone motion and environmental steering. *Mon. Wea. Rev.*, **109**, 908–909.

Chan, J. C.-L., 1982: On the physical processes responsible for tropical cyclone motion. Department of Atmospheric Science Pap. 358, Colorado State University, 200 pp.

——, and W. M. Gray, 1982: Tropical cyclone movement and surrounding flow relationships. *Mon. Wea. Rev.*, **110**, 1354–1374.

——, and R. T. Williams, 1987: Analytical and numerical studies of the beta-effect in tropical cyclone motion. Part I: Zero mean flow. *J. Atmos. Sci.*, **44**, 1257–1265.

DeMaria, M., 1985: Tropical cyclone motion in a nondivergent barotropic model. *Mon. Wea. Rev.*, **113**, 1999–2110.

Elsberry, R. L., 1986: Some issues related to the theory of tropical cyclone motion. Tech. Rep. NPS 63-86-005, Naval Postgraduate School, Monterey, CA, 23 pp.

Ferrel, W., 1859: The motion of fluids and solids relative to the earth's surface. *Math. Mon.*, **1**, 300–307.

Fiorino, M., 1987: The role of vortex structure in tropical cyclone motion. Ph.D. dissertation, Naval Postgraduate School, Monterey, CA, 93943, 370 pp.

George, J. E., and W. M. Gray, 1976: Tropical cyclone motion and surrounding parameter relationships. *J. Appl. Meteor.*, **15**, 1252–1264.

Gerald, C. F., and P. O. Wheatley, 1984: *Applied Numerical Analysis.* Addison-Wesley, 579 pp.

Holland, G. J., 1983: Tropical cyclone motion: Environmental interaction plus a beta effect. *J. Atmos. Sci.*, **40**, 328–342.

Kasahara, A., 1957: The numerical prediction of hurricane movement with the barotropic model. *J. Meteor.*, **14**, 386–402.

——, 1960: The numerical prediction of hurricane movement with a two-level, baroclinic model. *J. Meteor.*, **17**, 357–370.

Kuo, H.-L., 1969: Motions of vortices and circulating cylinder in shear flow with friction. *J. Atmos. Sci.*, **26**, 390–398.

Marks, F. D., and R. A. Houze, Jr., 1987: Three-dimensional structure of the eyewall of hurricane Norbert as determined from an airborne Doppler radar. Extended Abstracts, *17th Conf. on Hurricanes and Tropical Meteorology*, Miami, Amer. Meteor. Soc., 347–350.

Mathur, M., 1987: Development of NMC's high resolution hurricane model. Extended Abstracts. *17th Conf. on Hurricanes and Tropical Meteorology.* Miami, Amer. Meteor. Soc., 60–63.

Neumann, C. J., 1979: On the use of deep-layer-mean geopotential height fields in statistical prediction of tropical cyclone motion. Preprints, *Sixth Conf. on Probability and Statistics in Atmos. Sci.*, Banff. Amer. Meteor. Soc.

Rossby, C. G., 1948: On the displacement and intensity change of atmospheric vortices. *J. Mar. Res.*, **7**, 175–187.

Shuman, F., 1957: Numerical methods in weather prediction: II. Smoothing and filtering. *Mon. Wea. Rev.*, **85**, 357–361.

Tojo, S., 1953: The dynamics of a vortex embedded in a constant zonal current. *J. Meteor.*, **10**, 175–178.

Willoughby, H. E., 1988: Linear motion of a shallow-water, barotropic vortex. *J. Atmos. Sci.*, **45**, 1906–1928.

Yeh, T.-C., 1950: The motion of tropical storms under the influence of a superimposed southerly current. *J. Meteor.*, **7**, 108–113.